2019 19th International Conference on Control, Automation and Systems (ICCAS 2019)
Oct. 15∼18, 2019; ICC Jeju, Jeju, Korea

Damping Controller Design for Triangular Scanning of a Third-Order Nanopositioning Stage

Jie Ling[1,2], Tingting Ye[1], Zhao Feng[1,2], Min Ming[1], and Xiaohui Xiao[1,3*]

[1]School of Power and Mechanical Engineering,Wuhan University,
Wuhan, 430072, China. ({jamesling, tilda_ye, fengzhaozhao7, mingnmin_whu}@whu.edu.cn)
[2]National University of Singapore, Singapore, 119077, Singapore.
[3]Shenzhen Institute of Wuhan University,
Shenzhen, 518057, China. (xhxiao@whu.edu.cn) * Corresponding author

Abstract: In this paper, a design procedure of damping controller for third-order nanopositioning stage is presented for high-speed triangular scanning. Conventionally, damping control schemes of integral resonant control (IRC) and resonance-shifted IRC (RS-IRC) are designed providing that a second-order model can be identified for a nanopositioning stage. For a third-order system, existing control schemes cannot be applied directly. For this, a pole-zero cancellation technique is presented to design IRC scheme. In addition, a state observer based pole placement technique is proposed for RS-IRC design. The effectiveness of the proposed design procedures is demonstrated through both simulations and experiments based on a piezo-actuated nanopositioning stage platform. Results show that a closed-loop bandwidth of 156 Hz and 186 Hz are obtained by designed IRC and RS-IRC for the third-order nanopositioning stage, and the root-mean-square (RMS) errors of 40 Hz triangular tracking are 49 nm and 13 nm under IRC and RS-IRC control, respectively.

Keywords: Nanopositioning stage, Third-order system, Damping control, Integral resonant control, Observer design.

1. INTRODUCTION

Piezo-actuated nanopositioning stages are widely utilized to produce mechanical displacements with high resolution and high accuracy [1-3]. Owing to the merits of wide bandwidth, rapid response, and free friction [4, 5] of piezoelectric nanopositioning stages, successful applications can be found in abundant areas, including but not limit to scanning probe microscopy (SPM) [6, 7], micro electro mechanical systems (MEMS) [8], micromanipulators [9, 10], and data storage system [11]. However, the main challenge which restricts the motion speed lies in the lightly damped resonant modes of the compliant mechanism [3, 6-8, 11]. Unexpected structural vibrations may be easliy excited at relatively low frequencies, which results in a significant loss of positioning bandwidth of the stage.

To address the vibration issue, both feedforward and feedback control approaches have been investigated [12, 13]. Feedforward strategies, such as inversion-based compenstor [14], input shaping approach [15], iterative learning control with varying Q-filter [3], and iterative learning-based model predictive control [16], were proved effective in suppressing vibrational errors. An inherent drawback for a feedforward control approach is its high sensitivity to unmodelled dynamics and external uncertainties [12].

In view of that, various feedback schemes were proposed to damp the resonant modes. Some model-based methods like H_∞ control [17], linear quadratic Gaussian (LQG) control [6], output-feedback control using an interval model [2], and recursive delayed position feedback (RDPF) control [18] were reported. Low robustness of systems with low Q-factor and high order of the synthetic controller are some of the disadvantages that the aforementioned methods may suffer from. A class of fixed-structure low-order controllers based on the negative-imaginary theory was developed. This theory is broadly applicable to problems of robust vibration control for flexible systems with lightly damped modes [19]. Earlier research efforts such as resonant control (RC) [20], positive position feedback (PPF) [21], and positive velocity and position feedback (PVPF) [22] have been studied with substantial improved performance. The advantage of adopting fixed-structure low-order control schemes makes them practically implementable and computationally efficient.

For a collocated system, another negative-imaginary based approach named integral resonant control (IRC) is shown to be effective to damp multiple modes simultaneously in the presence of model uncertainty [23]. The parameters of IRC for a second-order system can be easily chosen using an analytical approach as discussed in [24]. To make further increase of the positioning bandwidth, a resonance-shifted IRC (RS-IRC) scheme has been proposed in [25] by shifting the resonant frequency using a negative unity feedback loop. An important assumption for the above negative-imaginary based controllers is that the nanopositioning system can be identified or reduced as a second-order dynamic model [20-22] or a sum of several second-order dynamic models [23-25]. However, a general dynamic model of a piezo-actuated nanopositioning stage is third-order as pointed out in [26]. This makes the design methodology of IRC and RS-IRC in [23-25] inapplicable for the nanopositioning stages with

This work was supported by the Project funded by China Postdoctoral Science Foundation under Grant No. 2018M642907, Shenzhen Science and Technology Program under Grant No. JCYJ20170306171514468 and Natural Science Foundation of China under Grant No.51375349.

third-order models.

Hence, the motivation of this paper is to extend the damping controllers from second-order systems to third-order systems by applying a pole-zero cancellation technique and a observer based pole placement technique for IRC nad RS-IRC design, respectively. To the best knowledge of the authors, few efforts have reported effective techniques for this issue except the PPF design for third-order systems in [26]. However, the structures of IRC and RS-IRC are totally different from that of PPF. We here propose the IRC and RS-IRC design procedures for fast tracking of a third-order nanopositioning stage, where the contributions are threefold: (1) a pole-zero cancellation technique is presented to design IRC for a third-order system; (2) a state observer based pole placement technique is proposed for RS-IRC design; (3) extensive experiments are conducted to evaluate the designed controllers based on a piezo-actuated nanopositioning platform.

The reminder of this paper is arranged as follows. Section II presents the experimental setup and the system identification. Section III briefly reviews the IRC and RS-IRC design procedures for second-order systems, and then the extension works of IRC and RS-IRC for a third-order system are discussed. Experimental results are shown in Section IV. Finally, Section V concludes this paper.

2. EXPERIMENTAL SETUP AND SYSTEM IDENTIFICATION

2.1 Experimental setup

Fig. 1 discribes the physical experiment system employed in this work. A commercial model of a piezo-actuated nanopositioning stage (model: P-561.3CD, from Physik Instrumente Co., Ltd.) is utilized to validate the proposed design methods of IRC and RS-IRC for three-order systems.

The signal flow of the control loop is shown in Fig. 1(b). For each axis, the control input voltage with a range of 0-10 V is produced by 16-bit digital to analog interfaces (DACs) of the data output module in real-time controller (model: MicroLabBox, from dSPACE Co., Ltd.). A piezo amplifier module (model: E-503.00, from Physik Instrumente Co., Ltd.) with a fixed gain of 10 amplifies the input vlotage and generates excitation voltage between 0 to 100 V. The output of each motion axis with a stoke of 100 μm, which is read by a PZT servo submodule (model: E-509.C3A, from Physik Instrumente Co., Ltd.), is subsequently passed to the data input module in dSPACE MicroLabBox with 16-bit analog to digital interfaces (ADCs). The control algorithm is designed in MATLAB/Simulink block diagram on the host PC, and then downloaded and executed on the target dSPACE MicroLabBox in the real-time software environment of dSPACE ControlDesk.

It should be noted that, in this work, only the z-axis in the vertical direction was utilized to implement the designed controllers for the nanopositioning system. The sampling frequency of the control loop was set as 10 kHz.

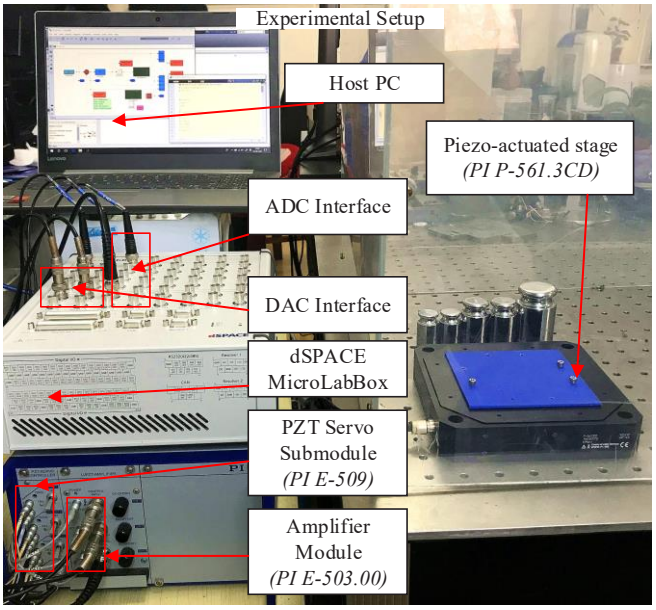

(a)

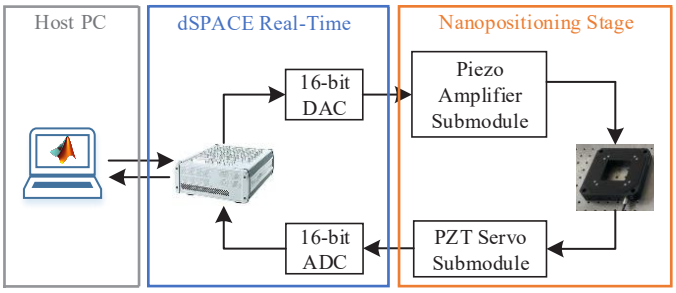

(b)

Fig. 1 Experimental setup of a piezo-actuated nanopositioning system: (a) experimental platform; (b) signal flow.

2.2 System identification

A chirp signal with a constant amplitude at 200 mV from 0 $\sim$ 500 Hz was fed into the z-axis. A low magnitude of input voltage was used here to avoid distortion from hysteresis. A linear time invariant (LTI) models from the input voltage to the output displacement of the axes are obtained using the Identification Toolbox of MATLAB, which can be shown as

$$G(s) = \frac{21.4s^2 - 8.45 \times 10^4 s + 2.93 \times 10^8}{(s + 250.5)(s^2 + 114s + 1.751 \times 10^6)} \quad (1)$$

where $G(s)$ stands for continuous transfer function from the input voltage $[V]$ to the output displacement $[\mu m]$ of z-axis.

The comparative bode digrams of the identified model and measured data are displayed in Fig. 2. It can be clearly found that the identified model accurately matches the measured dynamics of the system in the frequency range from 1 to 500 Hz. As discribed in (1), the real pole results in a drop before the resonant peak as can be seen in Fig. 2. This is the general bode diagram of a third-order nanopositioning system, which is quite different from second-order systems in [24] and [25]. Therefore, the design methods of IRC and RS-IRC in [24] and

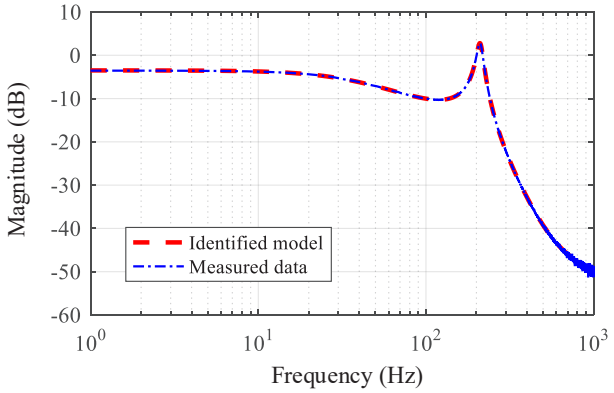

Fig. 2 Comparative bode digrams of the identified model and measured data.

[25] can not be directly adopted for the third-order system in this paper.

3. CONTROLLER DESIGN FOR THIRD-ORDER SYSTEMS

Before introducing damping controller design for third-order systems, a brief review of conventional IRC and RS-IRC schemes are presented in this section.

3.1 Conventional IRC and RS-IRC

As shown in Fig. 3a, the IRC scheme for second-order systems mainly consists of two loops. The inner positive feedback loop is utilized to damp the resonant peak so that the working bandwidth can be increased. A feedthrough term is added parallelly with the second order system to add a pair of zeros corresponding to the resonant poles. A damping controller C_d is designed and tuned to achieve a maximum damping ratio for the resonant peak. The outer negative loop is added to minimize the tracking errors especially in the low frequency range. Normally, an integral type C_t can be adopted. For the details of parameters' dertermination, readers can refer to the analysis in [24].

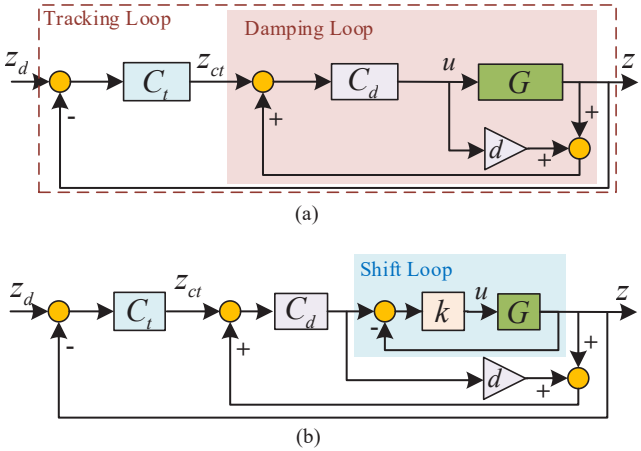

Fig. 3 Conventional IRC and RS-IRC schemes for second-order systems. (a) IRC; (b) RS-IRC.

On the basis of IRC scheme, the resonance-shifting integral resonant control scheme was proposed in [25]. Compared with Fig. 3a, an inner negative feedback loop is added for resonance-shifting. The shifter k is a positive gain which not only shifts the resonance peak but also increases the maximum peak value at the resonant frequency. The choice of k should make sure that the shifted resonance is within the sensor bandwidth as discussed in [25]. The remind parts of RS-IRC are the same with those of IRC.

The IRC has a better robustness performance than RS-IRC, while the bandwidth of is enhanced from IRC to RS-IRC. For the controller designers, a choice of IRC or RS-IRC can be made by evaluating the requirments for specific performance.

It should be noted that for third-order systems as described in (1), the IRC scheme can not be applied directly. In addition, the added shift loop in RS-IRC is always stable for a second-order system but unstable for a third-order system. Hence, the extension from second-order to third-order is meaningful for broadening the applications of IRC damping techniques.

3.2 IRC scheme for third-order systems

Inspired by the extension work of PPF in [26], we adopt the same operation that decomposing the third-order system G in (1) into a first-order system G_1 and a second-order system G_2 as,

$$G(s) = G_1(s) \cdot G_s(s) \qquad (2),$$

where $G_1(s) = \frac{k_1}{s+p_1}$, and $G_2(s) = k_2 \frac{s^2+2\zeta\omega_z s+\omega_z^2}{s^2+2\xi\omega_p s+\omega_p^2}$.

From previous studies of the authors, it is found that the second-order component G_2 dominates the final dynamic responses of G. In addition, the first-order component G_1 is insensitive to external uncertainties such as load variation, temperature change or micro disturbance, etc. Herein, for the identified first-order component G_1, a ploe-zero cancellation technique can be utilized to remove the effect of the first-order pole. As shown in Fig. 4, to keep the controller rational, a filter Q is added in both the two parallel feedthrough loops. A simple integral $Q = 1/s$ is utilized in this work to minimize the tracking errors in the inner damping loop.

Hereto, the original third-order system is reduced to a second-order system in the IRC scheme. The analytical approach in [24] can then be applied into the deisgn of remind parts in the modified IRC scheme for third-order systems.

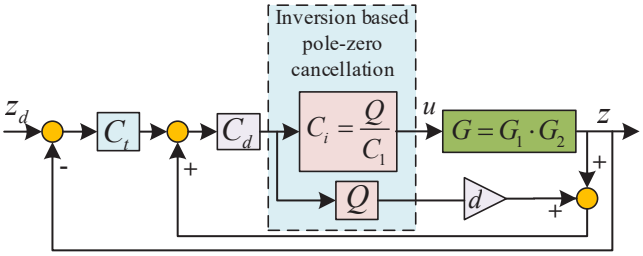

Fig. 4 Modified IRC scheme for third-order systems.

The design procedure for the proposed IRC for third-order systems can be summarized as follows:

- System decomposion as described in (2);
- Inversion based pole-zero cancellation using C_i and loop banlance configuration using filter Q;
- IRC design for $G_2(s)$ using the analytical approach in [24];
- Controller evaluations through simulations or experiments.

3.3 RS-IRC scheme for third-order systems

Different from the IRC scheme, RS-IRC contains a resonance shifting operation before the damping controller design. For a second-order system, a negative feedback gain can be utilized directly to shift the pair of conjugate poles as shown in the left of Fig. 6. However, if a third-system G with three poles is connected with a negative feedback gain k, the poles will lead to unstable poles as described through the right of Fig. 6. This can be easily derived by solving the characteristic equation of the closed-loop system $k \cdot G/(1 + k \cdot G)$.

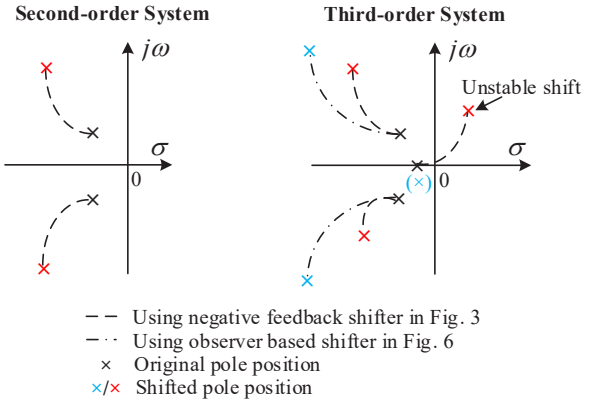

Fig. 5 Resonance shifting for second- and third-systems

Fot this, a state observer based shifter is proposed as depicted in Fig. 6. A main idea for this scheme is shifting the conjugate poles of G_2 to high frequency region while keeping the real pole of G_1 unchanged. This can be obtained by the well designed state observed. First, the objective pole positions of G_2 are set through shifting the orginal poles by -100 units or more. Second, a pole placement gain matrix K can be selected based on Ackermann's formula, which can be realized in MATLAB software using $acker$ command. Finally, the third-order system can be shifted to required status through a state observer as in Fig. 6.

The reminder of the RS-IRC scheme for third-order systems is similar to that of IRC scheme. Hereto, we present the summarized procedure of RS-IRC scheme as:
- System decomposion as described in (2);
- Set ideal pole positions of G_2 and keep the real pole position of G_1 unchanged;
- Calculate the pole placement gain matrix K using $acker$ command in MATLAB;
- Inversion based pole-zero cancellation using C_i and loop banlance configuration using filter Q;
- System decomposion for the shifted system and obtain the new second-order system $\widetilde{G}_2(s)$
- IRC design for $\widetilde{G}_2(s)$ using the analytical approach in [24];
- Controller evaluations through simulations or experiments.

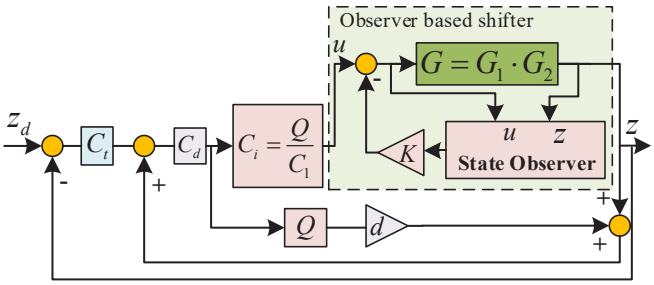

Fig. 6 Modified RS-IRC scheme for third-order systems.

4. EVALUATIONS

In this section, damping controllers of IRC and RS-IRC are designed based on the proposed procedures for a third-order system in (1). Both simulations and experiments are conducted for evaluations of the designed controllers.

4.1 Controller design results

4.1.1 IRC

Using the analytical approach in [24], IRC for G_2 is designed as,

$$d = -1.338, C_d(s) = 1.18 \times 10^3, C_t(s) = \frac{306}{s}, \quad (3)$$

and the inversion based cancellation filter is chosen as,

$$C_i(s) = \frac{s + 250.5}{250.5 \cdot s}, Q(s) = \frac{1}{s}. \quad (4)$$

4.1.2 RS-IRC

The designed results are,

$$d = -2, C_d(s) = 1.24 \times 10^3, C_t(s) = \frac{392.7}{s}, \quad (5)$$

and,

$$K = [6.59 \;\; 56.61 \;\; 26.81], C_i(s) = \frac{3.034s + 759.9}{250.5 \cdot s}. \quad (6)$$

4.2 Simulations for bandwidth test

Before experiments, the bandwidth and step responses the closed-loop system are tested through simulations.

As shown in Fig. 7, the designed controllers can achieve bandwidth enhancement. To be specific, closed-loop systems with IRC and RS-IRC result in a bandwidth of 156 and 186 Hz, respectively. A bandwidth improvement of 30 Hz is obtained by RS-IRC thanks to the resonance shifting based on the designed state observer compared with IRC.

The step responses are presented in Fig. 8. It can be found that both IRC and RS-IRC can converge to stable state within 0.02 s. The RS-IRC achieves shorter rising time and smaller overshoot than IRC, which is consistent with the results in Fig. 7 as RS-IRC results in larger bandwidth.

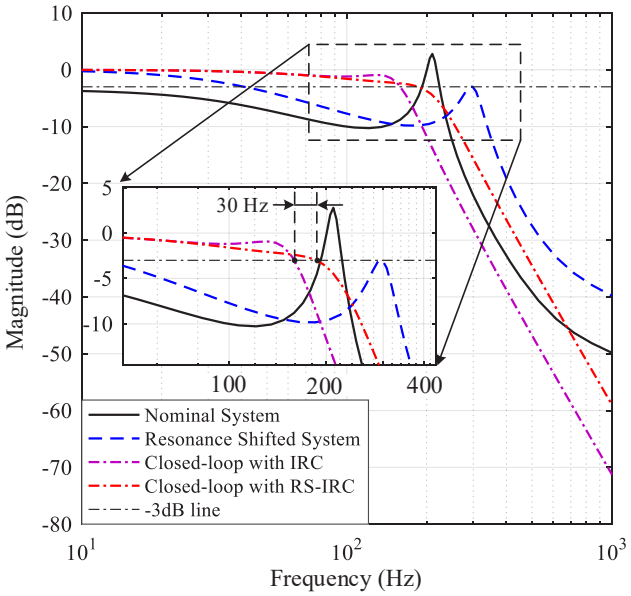

Fig. 7 Bandwidth test of open-loop and closed-loop systems with IRC and RS-IRC.

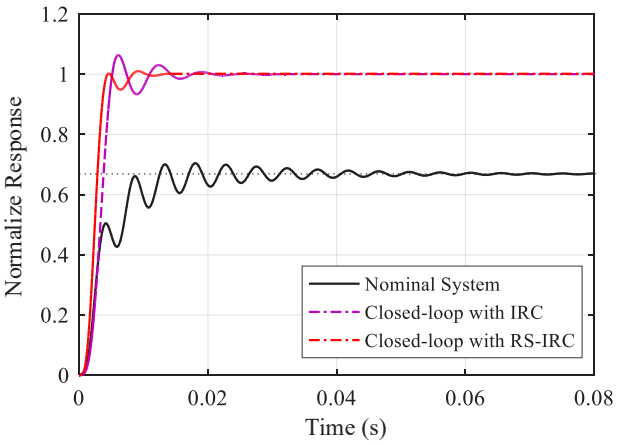

Fig. 8 Step responses of open-loop and closed-loop systems with IRC and RS-IRC.

4.3 Experiments for triangular tracking test

Triangular tracking is a common scanning mode for piezo-actuated nanopositioning in SPM. The triangular signal consists of a fundamental frequency and its odd harmonics, which are much higher than the fundamental frequency. Considering the achieved closed-loop bandwidth of the designed IRC and RS-IRC, 40 Hz triangular scanning is input for experiments.

Tracking results for both open-loop and closed-loop systems are recorded in Fig. 9. It can be seen that closed-loop with RS-IRC performs best among the three scenarios. The overshoot is evident for designed IRC as is consistent with the step responses in Fig. 8. The root-mean-square (RMS) errors for IRC and RS-IRC are 49 nm and 13 nm, where a 73% improvement is obtained from IRC to RS-IRC.

To sum up, based on the simulations and experiments, the proposed IRC and RS-IRC schemes in Fig. 4 and 6 are effective for a third-order nanopositioning stage.

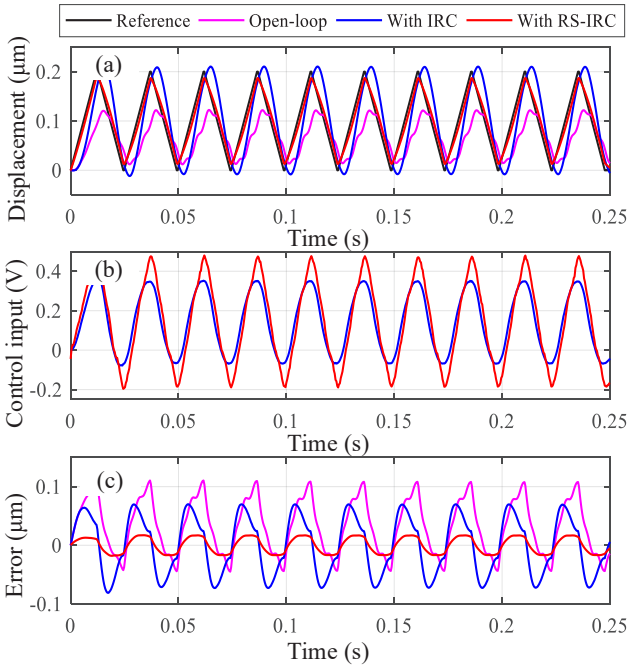

Fig. 9 Tracking results of 40 Hz triangular scanning of open-loop and closed-loop systems with IRC and RS-IRC.

5. CONCLUSIONS

The design procedures of IRC and RS-IRC for third-order nanopositioning systems are investigated in this paper. The main contributions are described in Fig. 4 and 6, where a pole-zero cancellation technique is proposed for IRC design and a state observer based pole placement technique is proposed for RS-IRC design. Detailed design procedures are also summarized for controller practisers. It should be noted that the proposed techniques are not only applicable for IRC and RS-IRC as proved through simulations and experiments in this paper, but also fit for other fixed-structure low-order damping controllers' design such as RC, PPF, PVPF etc.

REFERENCES

[1] Q. Xu, "Precision motion control of piezoelectric nanopositioning stage with chattering-free adaptive sliding mode control," *IEEE Transactions on Automation Science and Engineering*, Vol. 14, No. 1, pp. 238-248, 2017.

[2] J. Ling, Z. Feng, M. Ming, and X. Xiao, "Model reference adaptive damping control for a nanopositioning stage with load uncertainties," *Review of Scientific Instruments*, Vol. 90, No. 4, pp. 045101, 2019.

[3] Z. Feng, J. Ling, M. Ming, and X. Xiao, "High-bandwidth and flexible tracking control for precision motion with application to a piezo nanopositioner," *Review of Scientific Instruments*, Vol. 88, No. 8, pp. 085107, 2017.

[4] Z. Feng, J. Ling, M. Ming, and X. Xiao, "Data-based double-feedforward controller design for a coupled parallel piezo nanopositioning stage" *Proceedings of the Institution of Mechanical Engineers, Part I: Journal of Systems and Control Engineering*, Vol. 231, No. 10, pp. 881-892, 2017.

[5] Z. Wu, and Q. Xu, "Survey on recent designs of compliant micro-/nano-positioning stages," *Actuators*, Vol. 7, No. 1, pp. 5, 2018.

[6] H. Habibullah, H. R. Pota, and I. R. Petersen, "A novel control approach for high-precision positioning of a piezoelectric tube scanner," *IEEE Transactions on Automation Science and Engineering*, Vol. 14, No. 1, pp. 325-336, 2017.

[7] M. Ming, J. Ling, Z. Feng, and X. Xiao, "A model prediction control design for inverse multiplicative structure based feedforward hysteresis compensation of a piezo nanopositioning stage," *International Journal of Precision Engineering and Manufacturing*, Vol. 19, No. 11, pp. 1699-1708, 2018.

[8] J. Ling, M. Rakotondrabe, Z. Feng, M. Ming, and X. Xiao, "A robust resonant controller for high-speed scanning of nanopositioners: design and implementation," *IEEE Transactions on Control Systems Technology*, DOI. 10.1109/TCST.2019.2899566, pp. 1-8, 2019.

[9] Z. Feng, J. Ling, M. Ming, and X. Xiao, "Integrated modified repetitive control with disturbance observer of piezoelectric nanopositioning stages for high-speed and precision motion," *Journal of Dynamic Systems, Measurement, and Control*, Vol. 141, No. 8, pp. 081006, 2019.

[10] P. Wang, and Q. Xu, "Design and testing of a flexure-based constant-force stage for biological cell micromanipulation," *IEEE Transactions on Automation Science and Engineering*, Vol. 15, No. 3, pp. 1114-1126, 2018.

[11] J. Ling, Z. Feng, M. Ming, and X. Xiao, "Damping controller design for nanopositioners: a hybrid reference model matching and virtual reference feedback tuning approach," *International Journal of Precision Engineering and Manufacturing*, Vol. 19, No. 1, pp. 13-22, 2018.

[12] M. S. Rana, H. R. Pota, and I. R. Petersen, "A survey of methods used to control piezoelectric tube scanners in high-speed AFM imaging," *Asian Journal of Control*, Vol. 20, No. 2, pp. 1-21, 2018.

[13] G. Y. Gu, L. M. Zhu, C. Y. Su, H. Ding and S. Fatikow, "Modeling and control of piezo-actuated nanopositioning stages: a survey," *IEEE Transactions on Automation Science and Engineering*, Vol. 13, No. 1, pp. 313-332, 2016.

[14] K. K. Leang, and S. Devasia, "Feedback-linearized inverse feedforward for creep, hysteresis, and vibration compensation in AFM piezoactuators," *IEEE Transactions on Control Systems Technology*, Vol. 15, No. 5, pp. 927-935, 2007.

[15] S. S. Aphale, A. Ferreira,and S. R. Moheimani, "A robust loop-shaping approach to fast and accurate nanopositioning," *Sensors and Actuators A: Physical*, Vol. 204, pp. 88-96, 2013.

[16] S. Xie, and J. Ren, "High-speed AFM imaging via iterative learning-based model predictive control," *Mechatronics*, Vol. 57, pp. 86-94, 2019.

[17] O. Aljanaideh, and M. Rakotondrabe, "Observer and robust H-inf control a 2-DOF piezoelectric actuator equipped with self-measurement," *IEEE Robotics and Automation Letters*, Vol. 3, No. 2, pp. 1080-1087, 2018.

[18] C. X. Li, Y. Ding, G. Y. Gu, and L. M. Zhu, "Damping control of piezo-actuated nanopositioning stages with recursive delayed position feedback," *IEEE/ASME Transactions on Mechatronics*, Vol. 22, No. 2, pp. 855-864, 2017.

[19] I. R. Petersen, "Negative imaginary systems theory and applications," *Annual Reviews in Control*, Vol. 42, pp. 309-318, 2016.

[20] H. R. Pota, S. R. Moheimani, and M. Smith, "Resonant controllers for smart structures," *Smart Materials and Structures*, Vol. 11, No. 1, pp. 1-8, 2002.

[21] I. A. Mahmood, and S. R. Moheimani, "Making a commercial atomic force microscope more accurate and faster using positive position feedback control," *Review of Scientific Instruments*, Vol. 80, No. 6, pp. 063705, 2009.

[22] B. Bhikkaji, M. Ratnam, A. J. Fleming, and S. R. Moheimani, "High-performance control of piezoelectric tube scanners," *IEEE Transactions on Control Systems Technologys*, Vol. 15, No. 5, pp. 853-866, 2007.

[23] E. Pereira, S. S. Aphale, V. Feliu, and S. R. Moheimani, "Integral resonant control for vibration damping and precise tip-positioning of a single-link flexible manipulator," *IEEE/ASME Transactions on Mechatronics*, Vol. 16, No. 2, pp. 232-240, 2011.

[24] M. Namavar, A. J. Fleming, M. Aleyaasin, K. Nakkeeran, and S. S. Aphale, "An analytical approach to integral resonant control of second-order systems," *IEEE/ASME Transactions on Mechatronics*, Vol. 19, No. 2, pp. 651-659, 2014.

[25] M. Namavar, A. J. Fleming, and S. S. Aphale, "Resonance-shifting integral resonant control scheme for increasing the positioning bandwidth of nanopositioners," *Proc. of the European Control Conference*, pp. 1317-1322, 2013.

[26] C. X. Li, G. Y. Gu, M. J. Yang, and L. M. Zhu. Aphale, "Positive position feedback based high-speed tracking control of piezo-actuated nanopositioning stages," *Proc. of the International Conference on Intelligent Robotics and Applications*, pp. 689-700, 2015.